Heliyon 8 (2022) e10263

Contents lists available at ScienceDirect

Heliyon

journal homepage: www.cell.com/heliyon

Research article

Comparison of surface aspects of turned and anodized titanium dental implant, or abutment material for an optimal soft tissue integration

Attila Mühl [a], Péter Szabó [b], Olga Krafcsik [c], Zoltán Aigner [d], Judit Kopniczky [e], Ákos Nagy [f], Gyula Marada [f], Kinga Turzó [f,*]

[a] Private Dental Office, H-7300 Pécsi út 1., Komló, Hungary
[b] Szentágothai Research Center, Environmental Analytical and Geoanalytical Research Group, Ifjúság útja 20., H-7624, Pécs, Hungary
[c] Department of Atomic Physics, Budapest University of Technology and Economics, Budafoki út 8., H-1111, Budapest, Hungary
[d] Institute of Pharmaceutical Technology and Regulatory Affairs, Faculty of Pharmacy, University of Szeged, Zrínyi u. 9., H-6720, Szeged, Hungary
[e] Department of Optics and Quantum Electronics, University of Szeged, Dóm tér 9., H-6720, Szeged, Hungary
[f] Dental School, Medical Faculty, University of Pécs, Dischka Gy. u. 5., H-7621, Pécs, Hungary

HIGHLIGHTS

- Optimization of soft tissue barrier is a crucial factor in long-term dental implant success and peri-implant health.
- The applied anodization is an easy-to-use process to change the color of titanium to a more favorable yellow.
- Changes in surface morphology and hydrophilic features were favorable for soft tissue attachment.
- Anodized samples presented optimal surface composition to be used as abutment material of dental implants.

ARTICLE INFO

Keywords:
Titanium dental implant
Turned surface
Anodization
Gingival attachment
Roughness
Chemical composition
Contact angle

ABSTRACT

Objectives: Soft tissue integration of dental implants lags behind natural biological integration of teeth mainly because of non-optimal surface features. Peri-implant infections resulting in loss of supporting bone jeopardize the success of implants. Our aim was to compare an anodized surface design with a turned one for a more optimal surface.

Methods: Morphological and chemical structures of turned and anodized Ti surfaces (grade 5: Ti6Al4V) discs were examined by scanning electron microscopy (SEM-EDS), energy dispersive X-ray spectroscopy (EDS), and atomic force microscopy (AFM). The hydrophilic or hydrophobic features of the surfaces were determined by dynamic contact angle measurement.

Results: SEM and AFM revealed significant differences in the morphology and roughness (R_a) of the samples. Anodized discs presented a granular structure, while turned ones had circular grooves. The roughness was significantly higher for the anodized samples compared to the turned ones. XPS and EDS confirmed typical elements for both Ti6Al4V samples. Due to anodization, the amount of Ti (IV) had increased and Ti (III) had decreased in the thicker oxide layer. Anodized samples resulted in a more hydrophilic surface than the turned ones.

Significance: The results suggest that the tested anodized samples present optimal surface characteristics to be used as abutment material for an optimal soft tissue integration.

1. Introduction

Medicine uses different types of biocompatible medical devices to treat patients and improve their quality of life. Dental implants must face the unique challenge of breaking through the integument to the oral cavity in order to connect the prosthetic restoration with its endosteal anchorage. The oral environment is colonized by potential pathogens, threatening the health of peri-implant tissues. Failure of dental implants

* Corresponding author.
E-mail address: kinga.turzo@gmail.com (K. Turzó).

https://doi.org/10.1016/j.heliyon.2022.e10263
Received 6 April 2022; Received in revised form 6 July 2022; Accepted 8 August 2022

is caused mainly by peri-implant infections resulting in loss of supporting bone [1, 2, 3, 4]. Therefore, the optimization of soft tissue closure is a crucial factor in long-term implant success and peri-implant health.

The quality of the closure can be well described by the prevalence data of peri-implantitis [5]. The systematic review of Mombelli et al., shows that 10% of placed implants—and because patients can potentially receive multiple implants—20% of observed patients already within 5–10 years of placement, will face different grades of inflammation of peri-implant tissues. As a result of Mombelli et al., having selected the most relevant studies, performed by experienced researchers and including cooperative patients, longitudinal observation was made. In the study of Derks at al., non-selected patients who had received implants up to 9 years previously and were treated by doctors with different levels of professional experience were examined. 45% of patients presented different grades of peri-implantitis [6]. This high degree of prevalence demonstrates that soft tissue attachment around implants and abutments is not ideal in the biological width.

An endosteal implant anchored prosthesis can be divided to an intra-osseal, a transmucosal, and a supra-mucosal part. Peri-implant inflammation can be caused and also prevented by many factors, like tissue quality, biomaterial surface features, loading parameters, precision of odonto-technology, etc. Our investigation focuses on the quality of attachment on the transmucosal part of the surface of the endosteal anchored dental prosthesis. Two tissue types are involved in the soft tissue attachment of the implants. Connective tissue and epithelial attachment. The transmucosal part of the prosthesis can be a transmucosal area of a tissue level implant, an abutment, or the endosteal area of an implant which has already suffered bone loss or malpositioning. The material of the transmucosal section is crucial, therefore we should use just evidence based materials, supporting the optimal attachment of epithelium on its surface [7].

One of the most commonly used materials for dental implants is CP grade 5 titanium alloy, Ti6Al4V. It is biocompatible and its physical features make it a popular choice as an implant abutment. The quality of soft tissue attachment around a titanium abutment can be increased in a quantitative and qualitative way. One quantitative solution is to increase the transmucosal surface by creating curved shapes on prefabricated abutments. A more favorable solution is to utilize a custom emergence profile on individually fabricated elements. In thin soft tissue types, increased soft tissue height can also be a solution by submerged implant placement which can be developed by calculated the bone loss, within the framework of remodeling the bone [8].

A qualitative approach is the surface modification of titanium which can cause different soft tissue-titanium interaction. Topography, roughness, chemical composition, and surface free energy are the main factors determining the biocompatibility and the quality of soft tissue attachment [9, 10]. On the other hand, these parameters also affect the colonization and the competition for the surface of pathogenic factors. Different methods have been developed and utilized on transmucosal parts of implant and abutment surfaces in the dental industry with varying degrees of success [11]. This is why any kind of surface modification should be well investigated before *in vivo* utilization.

In the supra- and transmucosal region titanium has a disadvantage, owing to its gray color, especially in thin, soft tissue phenotypes [12].

An easy anodization process has been popular that can change the color of titanium to more favorable yellow or pink (Table 1). This method is also applied to help users in the identification of different implant components based on their color [13].

Anodization process of Titanium and its alloys is already well investigated, but it was not studied from the aspect of the quality of attachment on the transmucosal part of the surface of the endosteal anchored dental prosthesis. Anodization process is more examined from the aspect of osseointegration as seen in the publication of Alipal et al. [14].

Therefore, the main goal of our study was to investigate the physical changes of the titanium surface caused by the anodization process resulting in a yellow color and to compare it with turned surfaces. Scanning Electron Microscopy (SEM) and Atomic Force Microscopy (AFM) was utilized to visualize the surface structure, with AFM also being used for measurement of surface roughness (R_a) changes using various scales. Chemical composition was investigated through X-ray Photoelectron Spectroscopy (XPS) and Energy-dispersive X-ray spectroscopy (EDS) to measure surface and in-depth characteristics. Surface free energy was determined through dynamic contact angle (Θ) measurement.

2. Materials and methods

2.1. Sample preparation

Two different types of Ti surfaces were compared: the control surface was turned (turn milled) and the test one was anodized. The control samples (discs of 1.5 mm thick and 9 mm diameter) were cut from ASTM F136 grade 5 Titanium alloy rods (Denti System®, Hungary). The cutting method produced a surface roughness matching the criteria of an abutment, according to Bollen et al., verified through AFM measurements [15]. The test samples were cut from the same type of rod and an anodizing procedure was applied according to the Wieland Edelmetalle Gmbh. (Germany) protocol. The samples were immersed in acid Titanium Pickling Solution (Wieland Edelmetalle Gmbh. Germany) for 30 s, followed by cleaning in tap water, anodization by 52 V and 62 Ah for 180 s in Titanium Colouring Electrolyte (Wieland Edelmetalle Gmbh. Germany). Current has been provided by Power Station pe 1028 (Plating Electronic Gmbh. Germany). The discs were immersed in denatured alcohol for 25 s, followed by cleaning in tap water, drying by compressed air, cleaning with distilled water in ultrasound cleaner for 2 × 60 s and drying for 20 min.

Before all experiments, both anodized and control samples were cleaned with acetone, then with 70% ethanol for 15 min, and rinsed with ultrapure water three times.

2.2. Characterization methods

Surface topography was examined via SEM and AFM. Roughness (R_a) of the samples was determined with AFM. Chemical composition was investigated using XPS and EDS to measure surface and in-depth characteristics. Surface free energy was determined through dynamic contact angle (Θ) measurement.

2.2.1. SEM-EDS

Samples were analyzed with a Jeol JSM-IT500HR (Jeol, Tokyo, Japan) scanning electron microscope (SEM) equipped with a built-in energy dispersive X-ray spectrometer (EDS). Using the dry silicon-drift

Table 1. Color of Titanium depending on the anodization voltage (Wieland Edelmetalle Gmbh. Germany).

Anodization voltage (V)	Color
10–15	brown
20–25	lilac
30–35	bright blue
40	silver blue
55	yellow
70–80	pink
85	pinkish blue
90	turquoise
95	green
100	bright green

*The voltage values in this scale are to be taken as guidelines only, as they may vary in actual event.

(SDD) EDS detector enables fast and high accuracy elemental analysis [16, 17].

For the surface images, samples were coated with gold (Jeol JFC-1300 auto fine coater, Jeol, Tokyo, Japan) and the images were captured using secondary electron imaging mode and 5, 10 and 15 kV accelerating voltage. The morphological characteristics of the control and anodized discs were recorded at ×500, ×2000, ×5000, ×10000 and ×20000 magnifications and for better surface visualization were tilted at 45°.

2.2.2. AFM

For AFM a PSIA XE-100 instrument (PSIA Inc., South Korea) was utilized to examine the surface morphology and roughness (R_a) of the samples. AFM is a high-resolution imaging technique to study surfaces at the micron to nanometer scale, via a technique that measures forces on the AFM probe-tip as it approaches and retracts from the investigated surface. The tips were single-crystal silicon cantilevers (type: N, NSG30 series with Au reflective coating, resonant frequency 240–440 kHz, force constant 22–100 N/m) purchased from NT-MDT (Russia). The measurements were performed in tapping mode, with the height, deflection, and 3D images of area 40 μm × 40 μm, 20 μm × 20 μm and 7 μm × 7 μm were captured. R_a was determined using the AFM software program (with at least six independent measurements) as the arithmetic average of the surface height relative to the mean height.

2.2.3. XPS

Furthermore, the surface composition of the samples was examined through XPS, using a twin anode X-ray source (XR4, Thermo Fisher Scientific) and a hemispherical energy analyzer with a 9 channel multi-channeltron detector (Phoibos 150 MCD, SPECS). The base pressure of the analysis chamber was around 2×10^{-9} mbar. Samples were analyzed using a Mg K_α (1253.6 eV) anode, without monochromatization. Peak fitting was carried out using CasaXPS software. Wide-range scans and high-resolution narrow scans of the Ti 2p, O 1s, and C 1s characteristic peaks were recorded.

2.2.4. Dynamic contact angle (Θ) measurements

Contact angles were measured to examine the wettability of the surfaces of the control and anodized disc (4 samples for each disc). The wetting properties were investigated with the EasyDrop contact angle measuring system (EasyDrop K-100; Krüss Gmbh., Germany) with the sessile drop method. The measurements were carried out at 32.2 °C air and 35–36 °C sample temperature and contact angle values were determined dynamically over a period of 120 s following the drop of ultra-clean water having fallen on the surface of the disc.

2.3. Statistical analyses

The arithmetic means ± the standard error of the mean (SEM) were calculated for the R_a (nm) values measured by AFM. After normality testing, the data were compared via one-way analysis of variance (ANOVA), followed by Tukey's HSD, LSD and Scheffé post hoc tests to determine statistical differences after multiple comparisons (SPSS 21, SPSS, Chicago, Illinois, USA). The level of significance was set at $p = 0.05$.

3. Results

3.1. SEM images of the surfaces

SEM images (Figure 1) revealed considerable differences in the surface morphology and structure of the investigated samples. Turned (control) discs had circular grooves originating from the knife used in cutting the samples. The anodized Ti6Al4V discs exhibited typical, irregular surface characteristics with small grains of 0.1–3 μm size.

SEM images (Figure 1) at higher magnification (×5000) revealed the differences in the surface morphology and structure of the control and anodized samples.

The ×5000 magnification SEM image of the anodized surface reveals that the superficial granular layer covers the texture made by the turning procedure.

Additionally, we scratched the surface of both the control and anodized discs with the tip of a Titanium forceps to obtain information on the depth and characteristics of the underlying structure. SEM images were recorded at ×5000 magnification. The SEM image of the scratched turned sample showed the same surface characteristics as for the non-scratched turned sample, and the perpendicular cutting trace of the forceps on the milling lines were visible. In the case of the anodized samples, the SEM image shows that the scratching procedure removed the superficial granular structure and the underlying area was not like the turned surface. Deeper structures—valleys—were revealed, proving that the anodizing procedure had reached deeper regions of the sample. The scratching procedure was not a standardized procedure; therefore, the depth of surface change could not be determined. The EDS analysis provided additional data regarding the depth of the anodizing effect.

3.2. AFM images of the surfaces and determination of R_a values

AFM measurements provided information regarding the surface morphology and roughness (R_a (*nm*)) of the samples. Areas of 40 μm × 40 μm, 20 μm × 20 μm and 7 μm × 7 μm sample size were scanned.

AFM measurements of 7 μm × 7 μm and 20 μm × 20 μm areas provided important quantitative details regarding the size of the granular structures of the anodized samples (Figure 2).

The horizontal extent of the granules is around 1–2 μm and the vertical dimension is between 100–300 nm with a typical flat top. The same horizontal dimensions of the granules are visible on the SEM images at ×20000 magnification (Figure 2).

Figure 3 shows typical 3D AFM images of turned (control) and anodized Ti6Al4V samples measured at dimensions of 40 μm × 40 μm, 20 μm × 20 μm and 7 μm × 7 μm in size. These images demonstrate the different surface morphologies of the samples.

The quantitative measurement of roughness (R_a (nm)) of the samples using AFM provided results (Figure 4) that confirmed the differences in the surface pattern of the samples that were observed on the representative SEM images (Figure 1). There were also considerable variations in the roughness values of the different surfaces measured at different scanned sample sizes (Figure 4).

AFM measurements gave $R_a = 151 \pm 12$ nm for turned and $R_a = 158 \pm 9$ nm for anodized surfaces at the 40 μm × 40 μm sample size, with no significant difference ($p = 0.628$). These roughness values were produced by the wavy texture of the machining process, which was more pronounced over that of the anodized granular structure.

At the 20 μm × 20 μm sample size the anodized discs had significantly rougher surfaces ($R_a = 99 \pm 4$ nm) compared to turned discs ($R_a = 65 \pm 5$ nm; $p < 0.001$). At this field of measurement, grooves from cuts of the turned samples are visible, in a similar way as on the AFM images at 40 μm × 40 μm size. In the case of anodized samples, the typical granules dominate the field of view (FOV) over the grooves of cuts. Grooves are only detectable through targeting on the FOV at the boundary of the groove and the plane part of the samples.

AFM measurements at 7 μm × 7 μm sample size elicited considerable roughness differences ($p < 0.0001$): $R_a = 19 \pm 1$ nm for turned and $R_a = 87 \pm 4$ nm for anodized surfaces. Due to the small field of view, the grooves from cuts are completely undetectable and only minor burrs are visible on the turned samples. This is the reason for the significantly lower R_a values. In the case of anodized discs, the small FOV image shows a relatively flat surface with the presence of granules (100–300 nm in

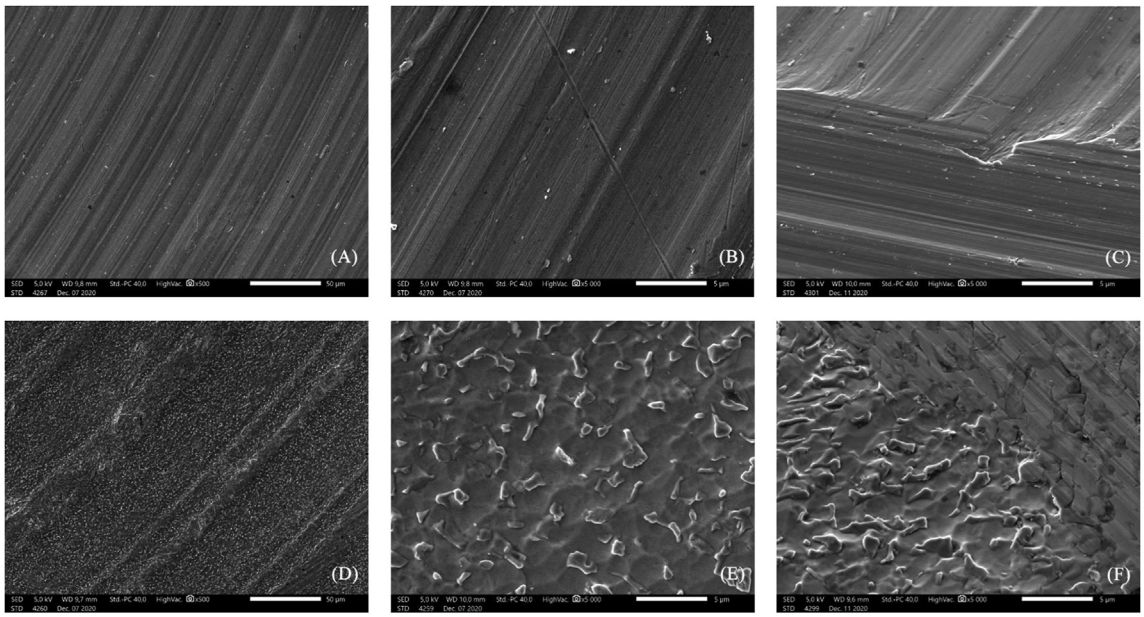

Figure 1. SEM images of the turned (A,B,C) and anodized (D,E,F) samples at ×500, ×5000 and scratched at ×5000 magnification (from left to right). Parts of circular grooves of the knife of the turn mill are visible, with small burrs on the turned surface. Small granules developed on the surface of circular grooves in the case of the anodized samples.

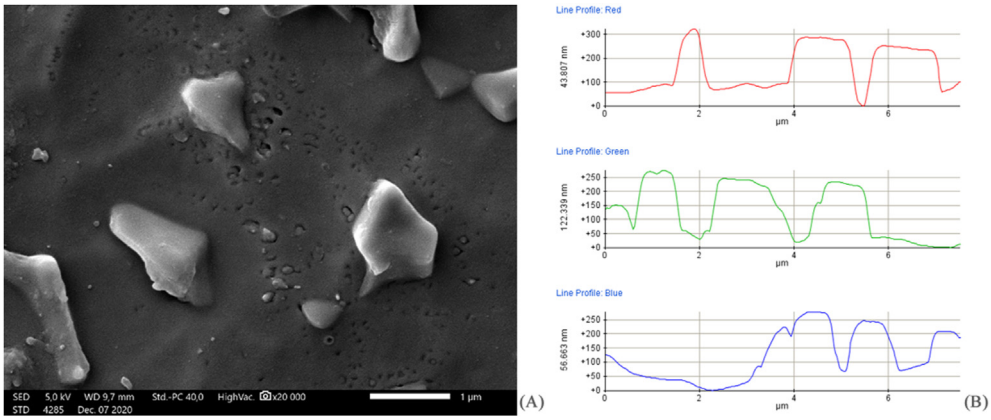

Figure 2. SEM image of the anodized sample at ×20000 magnification (A) and AFM line profiles of the anodized sample of a comparable 7 µm × 7 µm area (B).

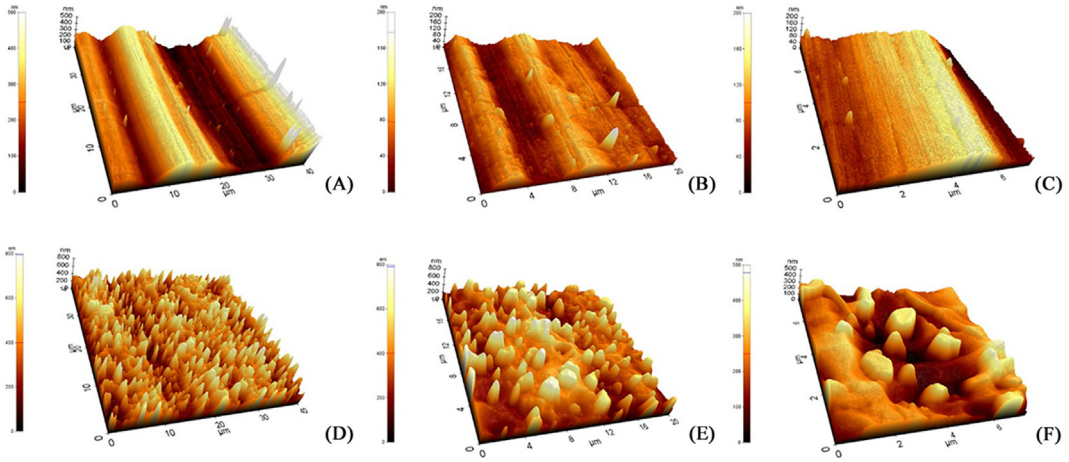

Figure 3. AFM 3D images of the turned (A,B,C) and anodized (D,E,F) samples of 40 µm × 40 µm, 20 µm × 20 µm and 7 µm × 7 µm areas (from left to right). The vertical scales of the images differ.

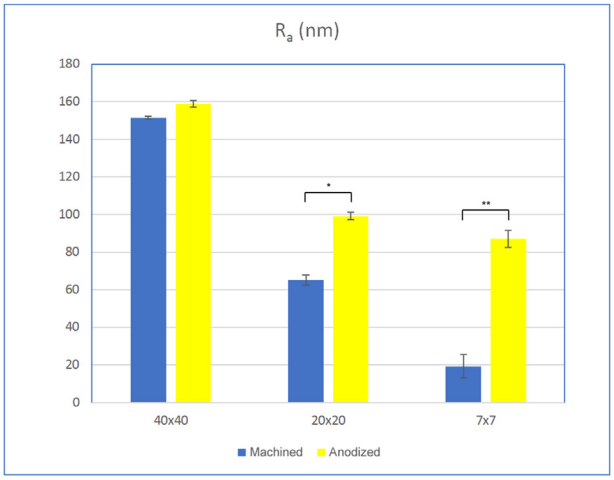

Figure 4. Average surface roughness values (R_a (nm)) of turned and anodized Ti6Al4V discs measured at 40 μm × 40 μm, 20 μm × 20 μm and 7 μm × 7 μm sample sizes. Data are given as means ± SEM. One-way ANOVA followed by Tukey's HSD post hoc test was utilized to determine the level of significance. Asterisks denote significant differences (*$p < 0.05$ and **$p < 0.0001$).

diameter and 1–2 μm in height). The major factor for the roughness is the granular texture produced during the anodization process.

A slight but significant difference could be observed between anodized samples measured (Figure 4) at 20 μm × 20 μm sample size ($R_a = 99 \pm 4$ nm) compared to 7 μm × 7 μm sample size ($R_a = 87 \pm 4$ nm; $p = 0.0275$).

3.3. XPS determination of surface chemical composition

X-ray Photoelectron Spectroscopy (XPS) and Energy-dispersive X-ray spectroscopy (EDS) makes possible the analysis and comparison of the chemical composition of the turned and anodized Ti6Al4V surfaces.

XPS survey spectra revealed C, O, Ti, Al, Ca, Cr, and N in the topmost atomic layers of both turned and anodized samples. The turned samples presented small amounts of F and Si, while anodized samples had P, Na, and Zn (Table 2).

Major changes of overall chemical composition were detected in the amount of carbon and oxygen (Table 2). The different carbon composition can be explained by the presence of carbonaceous contamination, due to C-containing molecules remaining after cleaning or adsorbed later on air-exposed surfaces. These elements are observed typically on Ti implant surfaces (NIST XPS Database) [18, 19].

Deconvolution of the Ti 2p peak gave the following results: the binding energy of Ti 2p 3/2 electrons, which corresponds to Ti^{4+}, was measured at 458.8 eV for turned sample and at 459.6 eV for the anodized sample. The double Ti peaks (Ti 2p at 458.8 and 464.6 eV) and the O 1s signal (~530 eV) confirm the presence of the TiO_2 layer [20]. The anodization process slightly changed the position of the Ti 2p 3/2 peak (459.6 eV) and a significant area increase occurred: 88.5% vs. 60.8% for the turned sample. An important modification can be seen in the Ti 2p 3/2 metal peak. The positions of the peaks are almost unchanged (453.9 eV for turned samples and 454.6 for anodized ones), but the area decreased significantly in the case of the anodized samples: 2.1% vs. 13.6% for the turned samples. samples (Figure 5).

Major changes were observed in the O 1s peak, which could be deconvoluted into three peaks. The most intense one, at ~ 530 eV, is that of lattice O in TiO_2; while the second most intense is between 533–534 eV, corresponding to the O in C–O and/or C=O bonds. The peak at ~ 532 eV is due to surface OH groups (Table 4). The significant change (almost 10 atomic %) in the oxygen content of the anodized surface compared to the turned one is due to the thickening of the oxide layer (Table 2). This finding is also supported by the deconvolution of the O 1s signal (Figure 5, Table 4).

The deconvolution of the C 1s signal (Table 5) produced three peaks for all samples. The most intense peak at ~ 285 eV is due to the C–C and C–H bonds. The peak at 287 eV corresponds to the C–O–C/C–OH groups—with minimal intensity difference (2.5%) between anodized and turned sample. The 289 eV binding energy value is a result of the O–C=O binding being present in approximately the same amount on the surfaces of the turned and anodized samples. The 2.2% difference can be caused by anodization, or due to different levels of contamination.

In general, anodization resulted in an increase in the prevalence of Ti (IV) —which is a component of TiO_2 molecules and TiOH groups (Tables 3 and 4). At the same time, due to anodization, the level of Ti (III) detectable in Ti_2O_3 molecules decreased (Tables 3 and 4).

3.4. EDS determination of surface chemical composition

In comparison with XPS, where detection depth is about 2–5 nm, EDS is more a bulk detection method with its up to 1 μm sampling depth. Figure 6 shows the EDS spectra and element analysis of turned and anodized discs. The deeper detection analysis leads to a lack of oxygen on the control disc, owing to the fact that the thin O layer is not detected at a greater depth (Figure 6). In the case of anodized samples, the atomic percentage of oxygen was 49, due to the higher thickness of the oxide layer produced by the electrochemical modification of the anodization process. This result is consistent with the findings of XPS (Tables 3 and 4) and SEM measurements (Figure 1). The images of the scratched anodized sample presented a deeper structure in comparison with the control surface.

3.5. Dynamic contact angle (Θ) measurements

Figure 7 shows the dynamic contact angle measurements of four turned and four anodized Ti6Al4V samples.

The mean contact angle (Θ) values of control discs ranged between 80.58°–69.07°, while for the anodized samples between 59.52°–39.62°. Anodization gave a significantly more hydrophilic surface compared to the turned samples.

4. Discussion

SEM and AFM demonstrated significant differences in the surface topography of the turned and anodized samples. Our study showed that

Table 2. Atomic percentage of typical elements on the surface of turned and anodized Ti6Al4V samples.

	Composition [at%]											
	C	O	Ti	Al	P	Ca	Na	Cr	F	Zn	N	Si
Turned	43.3	36.5	9.9	2.9	0	1.6	0	0.8	1	0	3	1
Anodized	33.1	46.2	11.1	1.5	4.7	1.5	0.1	0.6	0	0.1	1.2	0

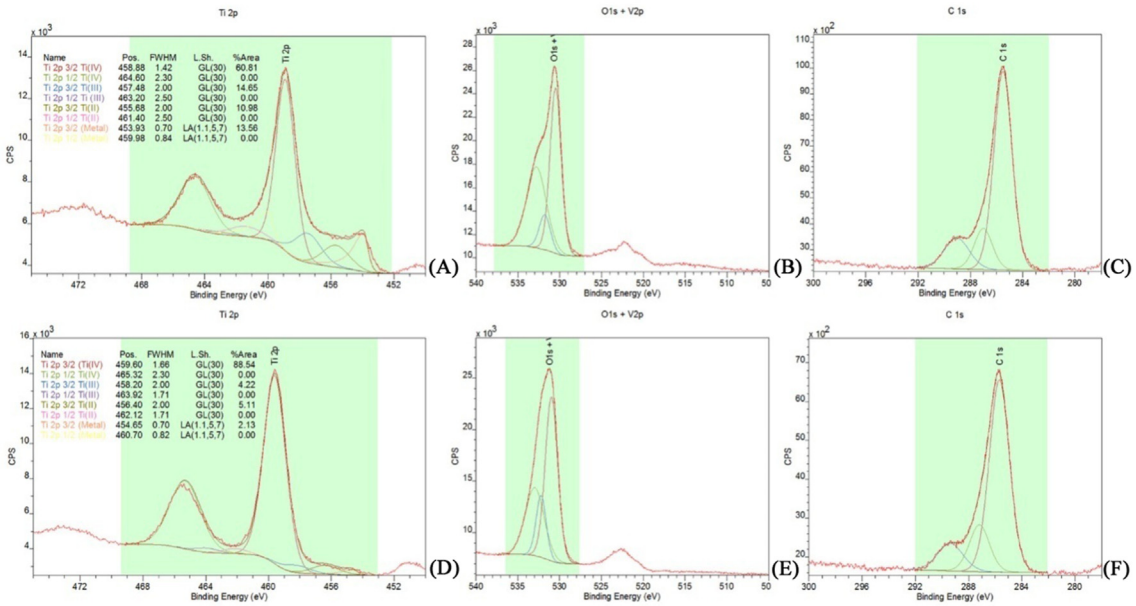

Figure 5. High-resolution XPS spectra showing Ti 2p, O 1s and C 1s signals (from left to right) of turned (A,B,C) and anodized (D,E,F) Ti6Al4V discs, confirming the presence of TiO_2 on all surfaces.

Table 3. Area (%)of Ti bonding states and location of the peaks measured by XPS on the surface of turned and anodized Ti6Al4V samples.

	Ti bonding state (%) ((Binding energy of the peak (eV))			
	Ti (IV)	Ti (III)	Ti (II)	Ti (Metal)
Control	60.8 (458.9 eV)	14.6 (457.5 eV)	11.0 (455.7 eV)	13.6 (453.9 eV)
Anodized	88.6 (459.6 eV)	4.2 (458.2 eV)	5.1 (456 eV)	2.1 (454.7 eV)

Table 4. Area (%) of O bonding states measured by XPS on the surface of turned and anodized Ti6Al4V samples.

	O bonding state (%)		
	Ti^{4+} - O	Ti^{3+} - O/C–O	O–H/C=O
Control	39.9	43.6	16.5
Anodized	52.1	15.6	32.3

Table 5. Area (%) of C bonding states measured by XPS on the surface of turned and anodized Ti6Al4V samples.

	C bonding state (%)		
	C–C/C–H	C–O–C/C–OH	O–C=O
Control	70.5	14.6	14.9
Anodized	70.2	17.1	12.7

surface roughness determined by AFM depends on the field of measurement due to the different macroscopic features of the surfaces. The turned samples typically presented grooves due to the concentric circles created by the turn mill which are most visible in the 40 μm × 40 μm sized images. For the anodized samples, the anodization process created a granular structure overlapping the original turned surface. AFM images measured at 20 μm × 20 μm and 7 μm × 7 μm sample sizes revealed these features and showed significant differences compared to the turned samples. In general anodization gave a rougher surface, but this surface is still within the range of the smooth surfaces (0.02–0.16 μm). The small granules of the anodized samples can be important for the cell adhesion during the soft tissue integration of the implant [21].

XPS and EDS confirmed typical elements and contamination free surface on both Ti6Al4V samples. Due to anodization thicker TiO_2 and TiOH was present, and the amount of Ti^{3+} had decreased on the surface. These characteristics are also preferred during soft tissue integration of implants [22].

Anodized samples rendered a significantly more hydrophilic surface than the turned ones. As underlined by Altankow et al. (1996) increasing wettability influences fibroblast attachment [23]. The level and speed of colonization by different pathogens can also be affected by the change in surface free energy [24, 25].

Our findings are consistent with the data published by Mussano at al. who investigated pink anodized Titanium alloy samples [26]. Their study showed a more superior fibroblast and epithelial cell attachment on the pink anodized surfaces. As these results are promising, we therefore plan to perform cell culture or *in vivo* studies with the yellow shaded anodized samples. Moreover, it is these modified Titanium alloys that are most commonly used in dental applications.

Furthermore, the modification of surface texture and wettability can influence the colonization of pathogens during the first healing period of dental implants [27]. Therefore, additional *in vivo* experiments are planned to evaluate the effect of the anodization process on the Ti surface in competitive environment between soft tissues and bacterial agents.

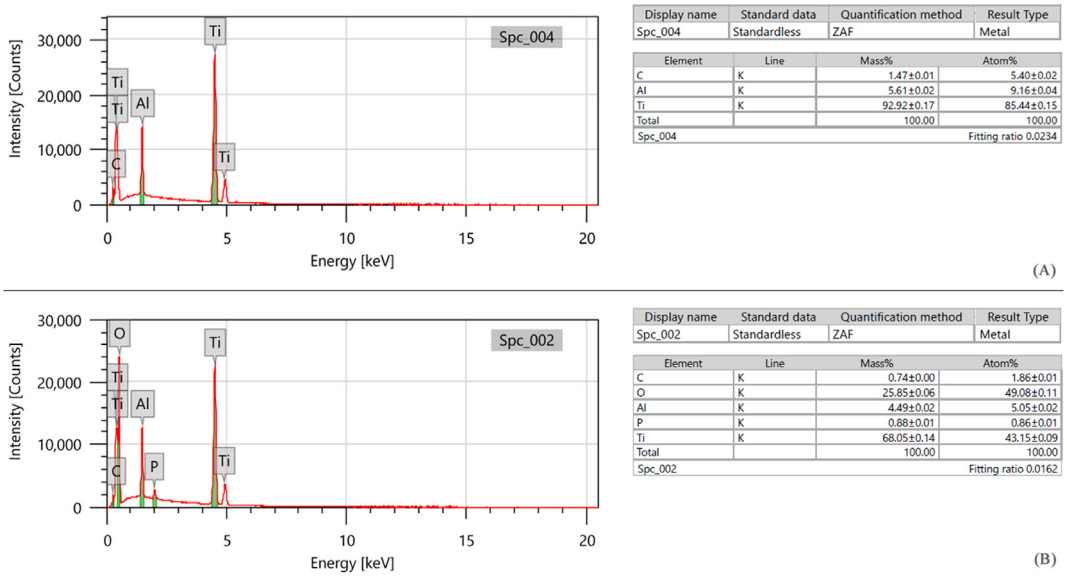

Display name	Standard data	Quantification method	Result Type
Spc_004	Standardless	ZAF	Metal

Element	Line	Mass%	Atom%
C	K	1.47±0.01	5.40±0.02
Al	K	5.61±0.02	9.16±0.04
Ti	K	92.92±0.17	85.44±0.15
Total		100.00	100.00
Spc_004			Fitting ratio 0.0234

Display name	Standard data	Quantification method	Result Type
Spc_002	Standardless	ZAF	Metal

Element	Line	Mass%	Atom%
C	K	0.74±0.00	1.86±0.01
O	K	25.85±0.06	49.08±0.11
Al	K	4.49±0.02	5.05±0.02
P	K	0.88±0.01	0.86±0.01
Ti	K	68.05±0.14	43.15±0.09
Total		100.00	100.00
Spc_002			Fitting ratio 0.0162

Figure 6. EDS spectra and element analysis of turned (A) and anodized (B) discs.

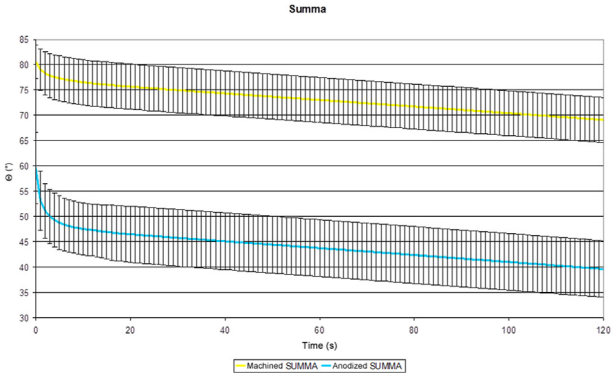

Figure 7. Summation of dynamic contact angle measurements of four turned and four anodized Ti6Al4V samples. The dynamic change of the mean contact angle for each samples are highlighted with yellow (turned sample) and blue (anodized samples) curves.

5. Conclusion

Anodization changed the morphological and roughness features of turned samples. Turned samples presented typical circular grooves due to the turn mill knife, while anodized samples had a granular structure. The roughness was higher for the anodized samples compared to the turned ones, most significantly for the lower FOV. XPS and EDS confirmed typical elements for both Ti6Al4V samples. Anodization resulted in an increase in the amount of Ti (IV) —which is a component of TiO_2 molecules and TiOH groups. Furthermore, in the anodized samples the level of Ti (III) detectable in Ti_2O_3 molecules decreased. Dynamic contact angle measurements displayed a more hydrophilic surface for the anodized samples than the turned ones.

In conclusion, the tested anodized samples present not just the best esthetic features but also the optimal surface characteristics to be used as abutment material to achieve an ideal soft tissue integration of dental implants.

Declarations

Author contribution statement

Attila Mühl; Kinga Kinga Turzó, PhD: Conceived and designed the experiments; Performed the experiments; Analyzed and interpreted the data; Contributed reagents, materials, analysis tools or data; Wrote the paper.

Péter Szabó, PhD; Olga Krafcsik, PhD; Zoltán Aigner, PhD; Judit Kopniczky, PhD; Ákos Nagy, PhD; Gyula Marada, PhD: Performed the experiments; Analyzed and interpreted the data; Contributed reagents, materials, analysis tools or data.

Funding statement

This research was supported by the project entitled "ÁOK-TANDEM_palyazat_2019_09_16_Turzó Kinga" sustained by the University of Pécs, Medical Faculty and co-funded by the National Research, Development, and Innovation Fund of Hungary under Grant TKP2021-NVA-02.

Data availability statement

Data included in article/supp. material/referenced in article.

Declaration of interest's statement

The authors declare no conflict of interest.

Additional information

No additional information is available for this paper.

Acknowledgements

We are grateful to Denti System® (Hungary) for providing the titanium sample discs.

References

[1] S. Renvert, A.-M. Roos-Jansaker, N. Claffey, Non-surgical treatment of peri-implant mucositis and peri-implantitis: a literature review, J. Clin. Periodontol. 35 (2008) 305–315.

[2] N.U. Zitzmann, T. Berglundh, Definition and prevalence of periimplant diseases, J. Clin. Periodontol. 35 (Suppl. 8) (2008) 286–291.

[3] P.A. Norowski Jr., J.D. Bumgardner, Review. Biomaterial and antibiotic strategies for peri-implantitis, J. Biomed. Mater. Res. Part B: Appl Biomater. 88 (2009) 530–543.

[4] V. John, D. Shin, A. Marlow, Y. Hamada, Peri-implant bone loss and peri-implantitis: a report of three cases and review of the literature, Case Rep. Dent. (2016), 2491714.

[5] A. Mombelli, N. Müller, N. Cionca, The epidemiology of peri-implantitis, Clin. Oral Implants Res. 23 (Suppl 6) (2012) 67–76.

[6] J. Derks, D. Schaller, J. Håkansson, J.L. Wennström, C. Tomasi, T. Berglundh, Effectiveness of implant therapy analyzed in a Swedish population: prevalence of peri-implantitis, J. Dent. Res. 95 (2016) 43–49.

[7] I. Abrahamsson, T. Berglundh, P.O. Glantz, J. Lindhe, The mucosal attachment at different abutments. An experimental study in dogs, J. Clin. Periodontol. 25 (1998) 721–727.

[8] T. Linkevicius, A. Puisys, R. Linkevicius, J. Alkimavicius, E. Gineviciute, L. Linkeviciene, The influence of submerged healing abutment or subcrestal implant placement on soft tissue thickness and crestal bone stability. A 2-year randomized clinical trial, Clin. Implant Dent. Relat. Res. 22 (2020) 497–506.

[9] B.D. Ratner, A.S. Hoffman, Thin films, grafts, and coatings, in: B.D. Ratner, A.S. Hoffman, F.J. Schoen, J.E. Lemons (Eds.), Biomaterials Science: An Introduction to Materials in Medicine, 309–312, Academic Press, San Diego, California, USA, 1996.

[10] H. Ananth, V. Kundapur, H.S. Mohammed, M. Anand, G.S. Amarnath, S. Mankar, A review on biomaterials in dental implantology, Int. J. Biomed. Sci. 11 (2015) 113–120. http://www.ncbi.nlm.nih.gov/pmc/articles/pmc4614011/.

[11] L. Canullo, M. Menini, G. Santori, M. Rakic, A. Sculean, P. Pesce, Titanium abutment surface modifications and peri-implant tissue behavior: a systematic review and meta-analysis, Clin. Oral Invest. (2020) 241113–241124.

[12] R. van Brakel, H.J. Noordmans, J. Frenken, R. de Roode, G.C. de Wit, M.S. Cune, The effect of zirconia and titanium implant abutments on light reflection of the supporting soft tissues, Clin. Oral Implants Res. 22 (2011) 1172–1178.

[13] T. Wang, L. Wang, Q. Lu, Z. Fan, Changes in the esthetic, physical, and biological properties of a titanium alloy abutment treated by anodic oxidation, J. Prosthet. Dent 121 (2019) 156–165.

[14] J. Alipal, T.C. Lee, P. Koshy, H.Z. Abdullah, M.I. Idris, Evolution of anodised titanium for implant applications, Heliyon 7 (2021), e07408.

[15] C.M. Bollen, W. Papaioanno, J. Van Eldere, E. Schepers, M. Quirynen, D. van Steenberghe, The influence of abutment surface roughness on plaque accumulation and peri-implant mucositis, Clin. Oral Implants Res. 7 (1996) 201–211.

[16] N.W. Ritchie, D.E. Newbury, J.M. Davis, EDS measurements of X-ray intensity at WDS precision and accuracy using a silicon drift detector, Microsc. Microanal. 18 (2012) 892–904.

[17] D.E. Newbury, N.W. Ritchie, Is scanning electron microscopy/energy dispersive X-ray spectrometry (SEM/EDS) quantitative? Scanning 35 (2013) 141–168.

[18] NIST XPS Database, Principal Photoelectron Lines Result, 2000.

[19] D.V. Kilpadi, G.N. Raikar, J. Liu, J.E. Lemons, Gregory JC. Vohra, Effect of surface treatment on unalloyed titanium implants: spectroscopic analyses, J. Biomed. Mater. Res. 40 (1998) 646–659.

[20] A.P. Ameen, R.D. Short, R. Johns, G. Schwach, The surface analysis of implant materials. 1. The surface composition of a titanium dental implant material, Clin. Oral Implants Res. 4 (1993) 144–150.

[21] E. Rompen, O. Domken, M. Degidi, A.E. Pontes, A. Piattelli, The effect of material characteristics, of surface topography and of implant components and connections on soft tissue integration: a literature review, Clin. Oral Implants Res. 17 (Suppl 2) (2006) 55–67.

[22] T.G. Donley, W.B. Gillette, Titanium endosseous implant-soft tissue interface: a literature review, J. Periodontol. 62 (1991) 153–160.

[23] G. Altankov, F. Grinnell, T. Groth, Studies on the biocompatibility of materials: fibroblast reorganization of substratum-bound fibronectin on surfaces varying in wettability, J. Biomed. Mater. Res. 30 (1996) 385–391.

[24] M. Lampin, Warocquier-Clérout, C. Legris, M. Degrange, M.F. Sigot-Luizard, Correlation between substratum roughness and wettability, cell adhesion, and cell migration, J. Biomed. Mater. Res. 36 (1997) 99–108.

[25] T.G. Ruardy, J.M. Schakenraad, H.C. van der Mei, H.J. Busscher, Adhesion and spreading of human skin fibroblasts on physicochemically characterized gradient surfaces, J. Biomed. Mater. Res. 29 (1995) 1415–1423.

[26] F. Mussano, T. Genova, M. Laurenti, E. Zicola, L. Munaron, P. Rivolo, P. Mandracci, S. Carossa, Early response of fibroblasts and epithelial cells to pink-shaded anodized dental implant abutments: an *in vitro* study, Int. J. Oral Maxillofac. Implants 33 (2018) 571–579.

[27] T. Wassmann, S. Kreis, M. Behr, R. Buergers, The influence of surface texture and wettability on initial bacterial adhesion on titanium and zirconium oxide dental implants, Int J Implant Dent 3 (2017) 32.